

Mesonic wavefunctions in the three-dimensional Gross-Neveu model

S.J. Hands^a, J.B. Kogut^b and C.G. Strouthos^a

^a *Department of Physics, University of Wales Swansea,
Singleton Park, Swansea, SA2 8PP, U.K.*

^b *Department of Physics, University of Illinois at Urbana-Champaign,
Urbana, Illinois 61801-3080, U.S.A.*

Abstract

We present results from a numerical study of bound state wavefunctions in the (2+1)-dimensional Gross-Neveu model with staggered lattice fermions at both zero and nonzero temperature. Mesonic channels with varying quantum numbers are identified and analysed. In the strongly coupled chirally broken phase at $T = 0$ the wavefunctions expose effects due to varying the interaction strength more effectively than straightforward spectroscopy. In the weakly coupled chirally restored phase information on fermion – anti-fermion scattering is recovered. In the hot chirally restored phase we find evidence for a screened interaction. The $T = 0$ chirally symmetric phase is most readily distinguished from the symmetric phase at high T via the fermion dispersion relation.

1 Introduction

Since the development of lattice gauge theory, many efforts have been made to measure the mass spectrum of hadrons. The spatial structure of hadrons, on the other hand, has not been as well-studied numerically, although experimentalists have measured quantities like the charge radius of the pion [1]. Numerical investigations of hadronic wavefunctions were initiated in 1985 by Velikson and Weingarten [2] and immediately afterwards they were followed by various other groups [3, 4]. Knowing the form factor of the hadrons would allow one to calculate their radii and higher moments. Hadronic wavefunctions are also useful in the calculation of masses because they can be used as trial wavefunctions in the construction of hadronic operators with improved overlap on the ground state at small Euclidean time separation. Furthermore, at high temperature DeTar pointed out the possibility of “confinement” at large distance scales [5]. Mesonic wavefunctions at non-zero temperature were investigated recently on an anisotropic lattice in the quenched approximation by the QCD-TARO Collaboration [6]. Their results suggest that above T_c there can be low energy excitations in the mesonic channels that are metastable bound states i.e. the quark and anti-quark tend to stay together at least for Euclidean time scales $\sim 1/T$. These quasiparticles would be characterized by a mass scale given by the location of a peak in the corresponding spectral function. This picture is consistent with mean field calculations in the Nambu–Jona-Lasinio model [7] which predict that the mesons associated with the chiral order parameter, namely the sigma and the pions are “soft modes” just above T_c , i.e. their fluctuations acquire a large strength with a small width in the spectral density, which implies the existence of long-lived quasiparticles. It has also been shown that the spatial wavefunctions for various mesonic channels in the high temperature phase [8, 9] are strongly localized, because of the nontrivial magnetic interaction of colour currents in the quark-gluon plasma.

In this paper we present results from a study of mesonic wavefunctions measured in numerical simulations of the $U(N_f)_V$ -invariant three-dimensional Gross-Neveu model (GNM₃) with both discrete Z_2 and continuous $U(1)$ chiral symmetries at both zero and non-zero temperature. The model with $U(1)$ chiral symmetry is described by the following semi-bosonized Euclidean Lagrangian density:

$$\mathcal{L} = \bar{\psi}_i(\not{\partial} + m_0 + \sigma + i\gamma_5\pi)\psi_i + \frac{N_f}{2g^2}(\sigma^2 + \pi^2). \quad (1)$$

We treat $\psi_i, \bar{\psi}_i$ as four-component Dirac spinors and the index i runs over N_f fermion species. In the case of a Z_2 chiral symmetry the π fields are set to zero in the Lagrangian. At tree level, the fields σ and π have no dynamics; they are truly auxiliary fields. However, they acquire dynamical content by dint of quantum effects arising from integrating out the fermions. The model is renormalizable in the $1/N_f$ expansion unlike in the loop expansion [10]. Apart from the obvious numerical advantages of working with a relatively simple model in a reduced dimensionality there are several other motivations for studying such a model: (i) at $T = 0$ for sufficiently strong coupling $g^2 > g_c^2$ it exhibits spontaneous chiral symmetry breaking implying dynamical mass generation for the fermion, the pion field π being the associated Goldstone boson; (ii) the spectrum of excitations contains both baryons and mesons, i.e. the elementary fermions f and the composite $f\bar{f}$ states; (iii) the model has an interacting

continuum limit at the critical value of the coupling, which has a numerical value $g^2/a \approx 1.0$ in the large- N_f limit if a lattice regularisation is employed [11]; (iv) numerical simulations of the model with chemical potential $\mu \neq 0$ show qualitatively correct behaviour, unlike QCD simulations [12, 13].

Let us briefly review the physical content of the model as predicted by the large- N_f approach [10, 11]. For $g^2 > g_c^2$ the fermion has a dynamically generated mass M_f equal, up to corrections of order $1/N_f$, to the scalar field expectation value $\langle \sigma \rangle = g^2 \langle \bar{\psi} \psi \rangle$. The inverse M_f^{-1} defines a correlation length which diverges as $(g^2 - g_c^2)^{-\nu}$ with the critical index $\nu = 1 + O(1/N_f)$. As a result of $f\bar{f}$ loop corrections the σ and π fields acquire non-trivial dynamics. In the case of the $U(1)$ -symmetric model, the pseudoscalar π couples to a Goldstone mode, and its propagator has a massless pole in the chiral limit $m_0 \rightarrow 0$. For both $U(1)$ and Z_2 chiral symmetries the scalar σ , by contrast, has mass $2M_f$ in the large- N_f limit, and rather than exhibiting an isolated pole, has a continuum of $f\bar{f}$ states extending all the way down to this threshold, implying that if truly bound, its binding energy is $O(1/N_f)$ at best. To our knowledge there have been no analytic calculations of the binding energy in this channel. Since all residual interactions are subleading in $1/N_f$, we surmise that all other mesons are similarly weakly bound states of massive fermions, and hence effectively described by a two-dimensional “non-relativistic quark model”. For $g^2 < g_c^2$ the model is chirally symmetric, and hence all states massless as $m_0 \rightarrow 0$. A dimensionful scale is still defined, however, by the width of a resonance in $f\bar{f}$ scattering in the scalar channel; this diverges as $(g_c^2 - g^2)^{-\nu}$ with the same exponent ν . In this case we have no equivalent of the quark model to assist interpretation of the wavefunctions to be discussed below.

The large- N_f approach [14] also predicts that for $g^2 > g_c^2$, chiral symmetry is restored as temperature T is raised beyond $T_c = M_f/2 \ln 2$, or for chemical potential $\mu > \mu_c = M_f$. The phase diagram of GNM₃ with various global symmetries at non-zero temperature and density has been studied extensively in [12, 13, 14]. More specifically, it has been shown that the thermally induced phase transition of the Z_2 -symmetric model belongs to the two-dimensional Ising universality class and the $U(1)$ -symmetric model undergoes a Berezinskii-Kosterlitz-Thouless transition [15] in accordance with the dimensional reduction scenario, which predicts that the long-range behaviour at the chiral phase transition is that of the $(d-1)$ spin model with the same symmetry, because the IR region of the system is dominated by the zero Matsubara mode of the bosonic field. An interesting aspect of GNM₃ is that it manifests both bulk and thermally-induced chirally-symmetric phases, and one of the goals of the present study is to compare and contrast their properties.

The shape and size of a hadronic state M can be observed through the equal time Bethe-Salpeter wavefunction given by:

$$\Psi(\mathbf{x}, t) = \int d\mathbf{y} \langle 0 | \bar{\psi}(\mathbf{y}, t) \psi(\mathbf{y} + \mathbf{x}, t) | M \rangle. \quad (2)$$

One can extract Ψ from the correlation function $C(\mathbf{x}, t)$ which is a convolution of the quark propagator G_q and the anti-quark propagator $G_{\bar{q}}$ and is given by:

$$C(\mathbf{x}, t) = \int d\mathbf{y} d\mathbf{y}_1 d\mathbf{y}_2 \langle 0 | \Phi(\mathbf{y}_1) \Phi(\mathbf{y}_2) G_q(\mathbf{y}, t; \mathbf{y}_1, 0) \Gamma G_{\bar{q}}(\mathbf{y} + \mathbf{x}, t; \mathbf{y}_2, 0) \Gamma | 0 \rangle \quad (3)$$

The Dirac matrix Γ selects the appropriate spin and parity quantum numbers for the meson, i.e., $\Gamma = \mathbf{1}$ for the spin zero scalar (S) and $\Gamma = \gamma_5$ for the spin zero pseudoscalar (PS). $\Phi(\mathbf{x})$

is an input trial wavefunction which is used as a source for the construction of quark and anti-quark propagators. At large t the contribution from the ground state dominates and

$$C(\mathbf{x}, t) \simeq \exp(-mt)\Psi(\mathbf{x}), \quad (4)$$

where m_H is the hadron mass. As already mentioned in [4] these wavefunctions are minimal Fock space wavefunctions, because they do not overlap onto states for which the quark anti-quark world line has kinks crossing time t . Therefore, their use to calculate phenomenological numbers is an uncontrolled approximation. However, as we shall see, they are convenient tools in lattice simulations to study the binding in the various mesonic channels. Due to its simplicity, the GNM₃ can be studied at both $T = 0$ and $T \neq 0$ on lattices with relatively large L_t , which is the main difficulty for QCD simulations. In the next section we will discuss numerical results of mesonic masses and wavefunctions on large volumes in both the scalar (S) and pseudoscalar (PS) channels. In our study we only measured the connected parts of the correlators. The noisy disconnected diagrams were neglected and we will discuss the implication of this in the next section. We will also discuss the dependence of our results on the quark propagator source, on the lattice spatial extent L_s , the chiral symmetry group (Z_2 vs. $U(1)$) of GNM₃, the coupling $\beta \equiv 1/g^2$ and the number of fermion species in the model N_f . We will then present results in the $T = 0$ and $T \neq 0$ symmetric phases. The sigma and the pion are represented in the semi-bosonised GNM₃ action by bosonic auxiliary fields and hence the correlation functions in these channels including disconnected diagrams can be measured with relatively high statistics. Unfortunately, the same technique cannot be applied to the wavefunctions which are point-split quark four-point functions. In another project, which in a sense is complementary to this one we are studying mesonic spectral functions including those of the auxiliary fields using the Maximum Entropy Method [16].

2 Simulations

The fermionic part of the lattice action we have used for the semi-bosonized GNM₃ with $U(1)$ chiral symmetry is given by [12]

$$\begin{aligned} S_{fer} &= \bar{\chi}_i(x) M_{ijxy} \chi_j(y) \\ &= \sum_{i=1}^N \left(\sum_{x,y} \bar{\chi}_i(x) \mathcal{M}_{xy} \chi_i(y) + \frac{1}{8} \sum_x \bar{\chi}_i(x) \chi_i(x) \left[\sum_{\langle \tilde{x}, x \rangle} \sigma(\tilde{x}) + i\epsilon(x) \sum_{\langle \tilde{x}, x \rangle} \pi(\tilde{x}) \right] \right), \quad (5) \end{aligned}$$

where χ_i and $\bar{\chi}_i$ are Grassmann-valued staggered fermion fields defined on the lattice sites, the auxiliary fields σ and π are defined on the dual lattice sites, and the symbol $\langle \tilde{x}, x \rangle$ denotes the set of 8 dual lattice sites \tilde{x} surrounding the direct lattice site x . The fermion kinetic operator \mathcal{M} is given by

$$\mathcal{M}_{xy} = \frac{1}{2} \sum_{\nu} \eta_{\nu}(x) [\delta_{y, x+\hat{\nu}} - \delta_{y, x-\hat{\nu}}] + m_0 \delta_{xy}, \quad (6)$$

where $\eta_{\nu}(x)$ are the Kawamoto-Smit phases $(-1)^{x_0+\dots+x_{\nu-1}}$, and the symbol $\epsilon(x)$ denotes the alternating phase $(-1)^{x_0+x_1+x_2}$. The auxiliary fields σ and π are weighted in the path

integral by an additional factor corresponding to

$$S_{aux} = \frac{N}{2g^2} \sum_{\tilde{x}} [\sigma^2(\tilde{x}) + \pi^2(\tilde{x})]. \quad (7)$$

The simulations were performed by using the standard hybrid Monte Carlo algorithm in which complex bosonic pseudofermion fields Φ are updated using the action $\Phi^\dagger(M^\dagger M)^{-1}\Phi$. Unless stated otherwise, the bare fermion mass m_0 was set to zero. According to the discussion in [12], simulation of N staggered fermions describes $N_f = 4N$ continuum species; the full symmetry of the lattice model in the continuum limit, however, is $U(N_f/2)_V \otimes U(N_f/2)_V \otimes U(1)$ rather than $U(N_f)_V \otimes U(1)$. At non-zero lattice spacing the symmetry group is smaller: $U(N_f/4)_V \otimes U(N_f/4)_V \otimes U(1)$. In the Z_2 -symmetric model the π fields are switched off and M becomes real. In this case according to the discussion in [11] simulation of N staggered fermions describes $N_f = 2N$ continuum species. Details about the algorithm and how we optimized its performance can be found in [11, 12].

Using point sources we calculated the zero momentum fermion correlator at different values of the coupling β and fitted to the function

$$C_f(t) = A_f[e^{-M_f t} - (-1)^t e^{-M_f(L_t - t)}]. \quad (8)$$

The mesonic correlators are given by:

$$C_M(t) = \sum_{\mathbf{x}, \mathbf{x}_1, \mathbf{x}_2} \Phi(\mathbf{x}_1)\Phi(\mathbf{x}_2)W_M(\mathbf{x})G(\mathbf{x}, t; \mathbf{x}_1, 0)G^\dagger(\mathbf{x}, t; \mathbf{x}_2, 0), \quad (9)$$

where $W_M(\mathbf{x})$ is a staggered fermion phase factor which picks out a channel with particular symmetry properties i.e. $W_M(\mathbf{x}) = \epsilon(x)$ for the S channel and $W_M(\mathbf{x}) = 1$ for the PS channel. The function $\Phi(\mathbf{x})$ is either a point source $\delta_{\mathbf{x},(0,0)}$ or a staggered fermion wall source $\sum_{m,n=0}^{L_s/2-1} \delta_{\mathbf{x},(2m,2n)}$ [17]. In all the simulations we used point sinks. These correlators were fitted to a function $C_M(t)$ given by

$$C_M(t) = A[e^{-mt} + e^{-m(L_t - t)}] + \tilde{A}(-1)^t[e^{-\tilde{m}t} + e^{-\tilde{m}(L_t - t)}]. \quad (10)$$

The first square bracket represents the “direct” signal with mass m and the second an “alternating” signal with mass \tilde{m} . Just as in four dimensions, composite operators made from staggered fermion fields project onto more than one set of continuum quantum numbers. To gain more insight one must transform to a basis with explicit spinor and flavor indices [18]; the resulting bilinears $\bar{q}(\Gamma \otimes T)q$ in both S and PS channels, where T acts on a two-component flavor space, are summarised in Table 1. Also shown are the spin/parity quantum

Table 1: Spin/flavor assignments of the fermion bilinears studied in the paper

| | $(\Gamma \otimes T)_{dir}$ | J_{dir}^P | $(\Gamma \otimes T)_{alt}$ | J_{alt}^P |
|----|---------------------------------|-------------|-------------------------------------|-------------|
| PS | $\gamma_5 \otimes \mathbf{1}$ | 0^- | $-i\gamma_1\gamma_2 \otimes \tau_3$ | 1^- |
| S | $\mathbf{1} \otimes \mathbf{1}$ | 0^+ | $i\gamma_0\gamma_3 \otimes \tau_3$ | 0^+ |

numbers J^P . In the direct channels these are the same as their four-dimensional equivalents,

but the alternating channels are very different. In the PS channel the alternating state is an anti-symmetric tensor, corresponding to spin-1, whereas in the S channel the bilinear transforms trivially under rotations in the 12 plane and is hence spin-0. The parity states are assigned by considering transformation properties under 2+1 dimensional lattice parity:

$$\begin{aligned}
x = (x_0, x_1, x_2) &\mapsto x' = (x_0, 1 - x_1, x_2) \\
\chi, \bar{\chi}(x) &\mapsto (-1)^{x_1+x_2} \chi, \bar{\chi}(x') \\
\sigma(\tilde{x}) &\mapsto \sigma(\tilde{x}') \quad ; \quad \bar{\pi}(\tilde{x}) \mapsto -\bar{\pi}(\tilde{x}').
\end{aligned}
\tag{11}$$

In continuum notation this corresponds to determining whether Γ commutes or anti-commutes with $\gamma_1\gamma_5$. It is important to note that unlike in 3+1 dimensions, the alternating channels do not contain “parity partners” of the direct channels, or indeed necessarily even describe states of the same spin.

In a similar way the lattice wavefunctions are given by:

$$\Psi(\mathbf{x}) = \sum_{\mathbf{x}', \mathbf{x}_1, \mathbf{x}_2} \Phi(\mathbf{x}_1)\Phi(\mathbf{x}_2)W_M(\mathbf{x})G(\mathbf{x} + \mathbf{x}', t; \mathbf{x}_1, 0)G^\dagger(\mathbf{x}', t; \mathbf{x}_2, 0).
\tag{12}$$

In the staggered formulation the easiest way to construct Ψ is by computing it for spatial separations that are multiples of $2a$. To facilitate comparison between the various wavefunctions we normalize them to unity at zero separation.

2.1 Zero Temperature Broken Phase

In this section we discuss the numerical results for the masses and the wavefunctions extracted from the S and PS channels of GNM₃ at $T = 0$. We generated statistics that vary from 700 to 2000 configurations, depending on how close to the critical point is the coupling for each simulation. The average molecular dynamics trajectory length $\bar{\tau} \simeq 1.2$.

First, we measured the meson correlators $C_M(t)$ in the S and PS channels and the fermion correlator $C_f(t)$ at different values of the coupling β from simulations of the Z_2 -symmetric model. An interesting observation is that the direct amplitude A in the S correlator is tiny compared to the alternating signal \tilde{A} , and appears to decrease rapidly as we decrease the coupling β , whereas the PS correlator is dominated by the direct signal. For example, in the case of the S correlator for $\beta = 0.75$ the fit parameters are $A = -0.00010(5)$, $\tilde{A} = 250(10)$, $\tilde{m} = 0.34(1)$, $M_f = 0.175(1)$ and for $\beta = 0.80$ they are $A = -0.05(1)$, $\tilde{A} = 235(5)$, $\tilde{m} = 0.172(1)$, $M_f = 0.0893(5)$. The bulk critical coupling is $\beta_c = 0.85(1)$. We infer that the alternating signal corresponds to a weakly bound state since its mass is slightly less than $2M_f$. It appears that the flavor-singlet scalar channel S_{dir} is completely dominated by disconnected diagrams in this phase, and can only be studied using the auxiliary σ field [11]. Because of the smallness of A in the S correlator (\tilde{A} in the PS correlator) for $\beta \lesssim \beta_c \simeq 0.85$, and the statistical fluctuations in our data we do not quote values for their masses; they did, however, appear very light, perhaps even consistent with zero, perhaps suggesting their origin is due to the proximity of the chirally symmetric phase at $\beta \gtrsim 0.85$.

Even in the case of continuous chiral symmetry, the meson extracted from the connected contribution in the PS_{dir} channel has a mass almost twice the fermion mass [13, 16] because

it is *not* the physical pion: the Goldstone mechanism in GNM_3 is fundamentally different from that in QCD. In this model the disconnected diagrams are responsible for making the pion light; numerically this can be accessed by studying correlators of the auxiliary π field [13, 16].

In Fig. 1 we present results for the PS channel wavefunctions of the Z_2 model with $N_f = 4$ on a $32^2 \times 96$ lattice and coupling $\beta = 0.55$. The wavefunctions were extracted from different timeslices ($t = 11, 21, 31, 41$) and were constructed from quark propagators with both wall and point sources. It is evident that the wavefunctions extracted from wall sources stabilize at relatively small Euclidean times. It is expected that the wall source projects onto the ground state much more effectively than the point source, because the wavefunction is very broad and it does not go to zero at the edge of the lattice, i.e. it resembles a wall wavefunction. The other advantage of the wall sources wavefunction is that it is constructed by convolving quarks with $\mathbf{p} = \mathbf{0}$, whereas the wavefunction extracted from point sources has more contamination from excited states at small times. As mentioned in the previous paragraph this weakly bound state has a mass which is very close to twice the fermion mass; in this case $M_{PS} = 1.085(3)$ and $M_f = 0.550(1)$. Because of the superior saturation properties, the various correlators that we will discuss in the next few paragraphs were constructed from wall sources.

In Fig. 2 we present PS_{dir} and S_{alt} wavefunctions at coupling $\beta = 0.55$ and lattice sizes $32^2 \times 96$ and $48^2 \times 96$. The wavefunctions fill the lattice even when $L_s = 48$ and it is obvious that finite size effects are still large at the boundary. In Fig. 3 we plot the S_{alt} and PS_{alt} wavefunctions in the broken phase for $\beta = 0.45, 0.55, 0.65$ with the horizontal axis rescaled by the fermion mass M_f which is an inverse correlation length. For small distances (in physical units $xM_f \lesssim 3$) the three PS_{dir} wavefunctions coincide, implying that in this regime the wavefunction shape is that of the continuum limit theory. We interpret the deviations at large distances as strong finite size effects; as implied by Fig. 2, the meson fills the lattice at these couplings. The S_{alt} wavefunctions which are broader than the PS_{alt} wavefunctions deviate slightly from each other even near the origin, indicative of stronger curvature in this region.

One clear effect is that the $f\bar{f}$ pair is much more closely bound in the PS channel than in the S. We can explain this by adapting the well-known argument from the non-relativistic quark model that a fermion – anti-fermion system bound in an s -wave is necessarily pseudoscalar due to the product of intrinsic parities of the $f\bar{f}$ pair being negative. Some care must be taken in 2+1 dimensions; whereas the $L = 0$ spatial wavefunction is axially symmetric and hence positive parity, all higher angular momentum states, which have the form $f(|\mathbf{r}|)e^{\pm iL\phi}$, where $f(r) \propto r^L$ for small r and for non-singular potentials, contain both positive and negative parity components (unlike in 3+1 dimensions where parity is given by $(-1)^L$), implying that higher spin states fall into degenerate parity doublets if parity is a good quantum number ¹. The conclusion remains, however, that the only allowed s -wave

¹Intrinsic parity must also be defined with care: recall that in 3+1 dimensions it is related to the spinor eigenstates of γ_0 . Since the continuum formulation of staggered fermions in 2+1 dimensions naturally results in 4-component spinors, we can effectively regard the parity transformation (11) as a spatial inversion in 3 dimensions followed by a rotation by π radians in the 23 plane; since rotations are continuous the f and \bar{f} spinor eigenstates maintain their respective intrinsic parities under this sequence of transformations.

state is the 0^- , which naturally accounts for why the PS_{dir} wavefunction has the smallest extent. The behaviour of states with $L > 0$ as a function of $|\mathbf{r}|$ might possibly explain the noticeable kink in the S wavefunction at the smallest non-zero spatial separation; ideally data nearer the continuum limit would be needed to explore this more thoroughly.

In Fig. 4 we present PS_{dir} and S_{alt} wavefunctions measured in simulations with different numbers of fermion species in the system, i.e., $N_f = 4, 12$. The coupling is set to $\beta = 0.55$ and the wavefunctions shown in this figure were extracted from the $t = 40$ timeslice. In order to compare the two cases and probe $1/N_f$ effects we rescaled the horizontal axis by multiplying the distance with the fermion mass M_f . It is clear from the figure that as we switch on the interaction (i.e. decrease N_f) the binding increases and the wavefunction shrinks. The ratio $M_{PS}/(2M_f)$ is 0.986(5) for $N_f = 4$ and 0.999(1) for $N_f = 12$. These results imply that the wavefunctions in this model are far more sensitive to $1/N_f$ effects than the masses or even the critical indices. In this model the bulk critical indices for finite N_f are very close to the large- N_f prediction and $1/N_f$ effects have been very difficult to measure even for relatively small N_f [19].

In Fig. 5 we present wavefunctions measured in the PS_{dir} and S_{alt} channels of GNM_3 with either a Z_2 or a $U(1)$ chiral symmetry. In both cases the number of fermion species is $N_f = 4$ and the coupling is $\beta = 0.55$. In the $U(1)$ model we fixed the vacuum by introducing a small fermion bare mass $m_0 = 0.01$ so that $\langle \sigma \rangle > 0$. The masses in the $U(1)$ model are: 1.133(3) for the S channel, 1.123(3) for the PS channel and 0.567(2) for the fermion. In the Z_2 model the masses are 1.085(5) for the S channel 1.083(5) for the PS channel and 0.550(2) for the fermion. These mesons have very broad but quite distinct wavefunctions, whereas their masses are almost the same and are very close to twice the fermion mass. This is further evidence that the wavefunctions in this model are more sensitive to binding effects than bound state masses. The difference between PS and S is larger in the $U(1)$ model than in the Z_2 model: the PS is more tightly bound, due to the additional attractive force resulting from π exchange, which since the π is lighter moreover also results in a longer-range $f\bar{f}$ potential. The kink in the S wavefunction is also more pronounced in this case. Although the various meson masses measured in our simulations are in accordance with the large- N_f prediction slightly less than $2M_f$, we believe that an accurate measurement of the binding energy can only be extracted from simulations on lattices which are bigger than the meson sizes, otherwise finite size effects can severely distort the result.

2.2 Zero Temperature Symmetric Phase

We now consider the wavefunctions in the chirally symmetric phase. As discussed in the Introduction, here there is no dynamically generated mass scale, and no readily identifiable correlation length, although evidence for a resonance width μ scaling approximately linearly in $(g_c^2 - g^2)$ was reported in [11]. In Fig. 6 we show the PS_{dir} wavefunctions of the Z_2 model in both broken ($\beta < \beta_c$) and symmetric ($\beta > \beta_c$) phases. The main observation is that the wavefunction becomes broader, i.e. the size of the meson increases, as β increases, but that some $f\bar{f}$ attraction persists beyond the critical point $\beta_c = 0.85(1)$. Counterintuitively, the wavefunction size in lattice units continues to increase for $\beta > \beta_c$, whereas the correlation length should decrease as we recede from the critical point. This may indicate that there is no

true bound state in the channel, but merely a positive spatial correlation due to interparticle attraction, which grows weaker as $\beta \rightarrow \infty$. Before taking this interpretation too seriously, however, it should be remarked that taken on their own the data of Fig. 6 would not enable the critical coupling to be identified.

In Fig. 7 we plot data extracted from a simulation on a 32^3 lattice at coupling $\beta = 1.0$ in the symmetric phase in both S and PS channels. We generated 10,000 configurations. A simple analysis of the correlators $C_M(t)$ implies that both are massless. Compared with the broken phase, however, the saturation is much improved, permitting a more complete analysis, which ultimately permits extraction of both direct and alternating signals from each channel. It is possible that in this case the wavefunction is yielding information on particle scattering rather than on an isolated bound state – this may explain the improved saturation, since there is no longer a requirement for the signal from excited states to die away as t increases before the shape of $\Psi(x)$ stabilises.

We disentangled $\Psi_{dir}(x)$ and $\Psi_{alt}(x)$ by measuring $\Psi(x, t)$, which is given by

$$\Psi(x, t) = A\Psi_{dir}(x) + (-1)^t \tilde{A}\Psi_{alt}(x), \quad (13)$$

at large even and odd t . The results presented in Fig. 7 were extracted by from the values of Ψ at $t = 14, 15$. A striking feature of the plot is that $|\Psi_{PS}| + |\Psi_S|$ appears independent of x . In fact, the meson amplitudes are of opposite signs, implying that the sum of factors $W_{PS} + W_S$ (see (12)) is of the form $(1 - \epsilon(x))$ and hence projects onto odd sink lattice sites only. Now, in a chirally symmetric vacuum, meson states built from non-interacting fermions (implying a spatially uniform Ψ) have contributions of precisely this form $G_{oe}G_{oe}^\dagger$; quantum corrections to $|\Psi_{PS}| + |\Psi_S|$ can therefore only arise from exchange of an even number of auxiliary bosons, and hence are suppressed by $O(1/N_f^2)$ at least. As already observed the PS wavefunctions expand as we increase β , with PS_{dir} more tightly bound than PS_{alt} . The similarity in shape may indicate that according to the assignments of Tab. 1 both are permitted to scatter in the s -wave. In contrast to the PS case, there *is* a qualitative difference in S channel wavefunctions between broken and symmetric phases. The wavefunction in both S_{dir} and S_{alt} *increases* away from the origin, implying that close approach of the $f\bar{f}$ is disfavoured. This is consistent with the requirement of positive parity states to have non-zero orbital angular momentum.

2.3 Nonzero Temperature

Next we discuss the effects of non-zero temperature T . We have studied lattices with temporal extent $L_t = 16$, for which the critical point for the Z_2 symmetric model is estimated to be $\beta_c^T = 0.790(5)$ [15], and the high temperature chirally restored phase can thus be studied for $\beta_c^T < \beta < \beta_c^{bulk}$. A particular virtue of GNM₃ is that, unlike unquenched QCD, it permits a study of hot dynamics with current resources with L_t sufficiently large to permit the measurement of thermal masses from correlators in Euclidean time. We have extracted the thermal fermion mass M_f^{th} by fits to

$$C_f(t) = A(1 - (-1)^t) \sinh(M_f^{th}(t - L_t/2)) + B(1 + (-1)^t) \cosh(M_f^{th}(t - L_t/2)). \quad (14)$$

We performed simulations on $32^2 \times 16$ and $96^2 \times 16$ lattices and we generated approximately 20,000 configurations on the smaller lattice and 35,000 on the bigger one. However, our data are consistent with the vanishing of $C_f(t)$ for even t , corresponding to $B = 0$ in (14), signalling a manifest chiral symmetry. The results for M_f^{th} are given in Tab. 2. We observe

Table 2: Thermal fermion masses in the hot phase

| β | $32^2 \times 16$ | $96^2 \times 16$ |
|---------|------------------|------------------|
| 0.79 | – | 0.048(1) |
| 0.80 | 0.044(1) | 0.041(1) |
| 0.82 | – | 0.034(1) |
| 0.85 | 0.026(1) | – |

that M_f is reasonably insensitive to the spatial volume of the lattice. The masses, though small, are considerably larger than those extracted from the bulk symmetric phase on a 32^3 lattice, where typical values found were $M_f = 0.006(1)$ at $\beta = 1.0$ and $0.0015(3)$ at $\beta = 2.0$, ie. virtually massless. The fermion mass thus provides a criterion from distinguishing the two chirally symmetric phases. In thermal field theory the typical scale for thermal masses is given by $m^{th} \sim g(T)T$ where $g(T)$ is the coupling strength associated with a vertex in a perturbative calculation. For GNM₃ the coupling associated with the UV fixed point is [11]

$$g = \frac{4}{N_f \sqrt{k^2}}. \quad (15)$$

For asymptotically high T we thus have $g(T) \propto T^{-1}$ and hence $\lim_{T \rightarrow \infty} M_f^{th} \rightarrow \text{const.}$ For finite T we still expect M_f^{th}/T to increase more slowly than T , implying that for fixed L_t $M_f^{th}a$ should decrease as $\beta \rightarrow \beta_c^{bulk}$, as suggested by the data of Tab. 2. In this limit the large- N_f expansion suggests that GNM₃ becomes an ideal fermi gas [20].

We have also examined fermion correlation functions at non-vanishing momenta $\mathbf{k} = 2\pi\mathbf{n}/L_s$, $n = 0, 1, 2, \dots$ and used the energies $E(k)$ extracted from (14) to map out the fermion dispersion relation. Results from both hot and bulk chirally symmetric phases are shown in Fig. 9, together with fits to the lattice form

$$E(k) = A \sinh^{-1}(\sqrt{\sin^2 k + M_f^2}). \quad (16)$$

The fits yield masses consistent with those extracted by fitting directly at zero momentum, and in both phases yield values of A , related to the renormalised speed of light, very close to 1, implying that the principal physical effect of the hot medium is to generate a non-zero thermal mass. A similar observation has been made in quenched QCD [9]. The result $A \simeq 1$ supports our identification of a non-zero screening mass, or “pseudogap”, in studies of the $U(1)$ -symmetric model at $T > 0$ [15], where large volume effects precluded using L_t sufficiently large to extract $E(k)$. Modifications of the low momentum part of the dispersion relation which is expected to have two branches at $T > 0$ [21] corresponding to two kinds of quasiparticle excitations, the fermion and the hole (known as the plasmino), are not visible in our simulations. Much larger lattices are needed to study the structure of the dispersion relation at the required low momenta.

As in the bulk symmetric phase, it is necessary to have accurate measurements of meson masses before wavefunctions can be extracted. On 16×32^2 at $\beta = 0.80$ we found a mass 0.075(5) in the PS_{dir} channel, which decreased to 0.038(3) at $\beta = 0.85$, and masses close to if not consistent with zero for PS_{alt} . In the S channel stable signals were found in both S_{alt} (0.090(2)) and S_{dir} (0.047(2)) at $\beta = 0.80$, decreasing to 0.051(5) and 0.037(5) by $\beta = 0.85$. As in the bulk symmetric phase, saturation was found to be quite satisfactory, which may again be a sign that there is no bound state pole. The resulting wavefunctions in PS_{dir} and PS_{alt} channels are shown in Fig. 8. The general shapes are very similar to those seen in both chirally broken and bulk symmetric phases, with the width of the wavefunction increasing monotonically with β . In principle the x axis should be rescaled with the correlation length given by $M_f^{-1}(T = 0)$; however, we have not done so since $\beta = 0.85$ is extremely close to the bulk critical point where finite volume corrections are large, making an estimate of $M_f(T = 0)$ by any other means than naively extrapolating from smaller β using $\nu \simeq 1$ impracticable. Instead, we note that the physical scale of the structure in Fig. 8 must shrink to zero as $\beta \rightarrow \beta_c^{bulk}$, implying that the region where $f\bar{f}$ interactions are important becomes pointlike as $T \rightarrow \infty$. This could perhaps be explained in terms of Debye screening of the $f\bar{f}$ interaction due to thermal effects. Once again, we are unable to determine the issue of whether the mesons remain bound states for $T > T_c$ without a detailed study of the spectral function – the behaviour of $\Psi(x)$ for large x is subject to large finite volume effects in this coupling regime.

3 Summary and Outlook

We have applied a technique originally developed for studying mesons in QCD, namely analysis of spatial wavefunctions, in a simpler model which manifests a variety of interesting behaviours as both coupling strength and/or temperature are varied. We have successfully identified mesonic bound states in the chirally broken phase, and exposed the effects of changing the strength of the interaction, either by altering the number of species N_f or the chiral symmetry group, much more cleanly than permitted by a study of the spectrum alone. The physical picture is a two-dimensional analogue of the quark model, with the s -wave nature of the PS state clearly distinguishable. Since the states are weakly bound, they have a larger spatial extent than the corresponding QCD mesons, and hence are more prone to finite volume corrections. We have also studied the wavefunctions in two distinct chirally symmetric phases, a $T = 0$ phase for $\beta > \beta_c^{bulk}$, and a hot phase for $\beta_c^T < \beta < \beta_c^{bulk}$. Because of the difficulties in reliably extracting a correlation length in either case, our study here has necessarily been more exploratory. Nonetheless we have seen evidence for a clear channel dependence in the spatial correlation of propagating $f\bar{f}$ pairs, which may now be due to a continuum of scattering states rather than isolated bound states. Interestingly, the clearest distinction between the two symmetric phases comes from a study of the fermion dispersion relation, which yields a non-vanishing thermal mass for the $T > 0$ study. If we use our expectations from the large- N_f approach, then the wavefunctions also provide evidence for screening in the hot phase.

The difficulties we have faced with finite volume effects are intimately related to the details of the spectrum of the model. In a related study [16] we are analysing the spectral

functions of the model using Maximum Entropy techniques. One advantage is that this approach permits analysis of the auxiliary fields, corresponding in lattice QCD parlance to the inclusion of disconnected quark line diagrams as well. It is hoped that this complementary approach will also help to resolve the issue of whether there are bound states in the chirally symmetric phases.

Finally, another feature of GNM₃ is that it permits simulation with a non-zero chemical potential μ , making studies of degenerate “quark matter” possible [14]. We are currently extending our wavefunction studies to $\mu \neq 0$, where a sharp Fermi surface manifests itself by a $\Psi(x)$ which fluctuates in sign, demonstrating so-called Friedel oscillations [22].

Acknowledgements

Discussions with Chris Allton are greatly appreciated. SJH and CGS were supported by a Leverhulme Trust grant, and also partially by EU TMR network ERBFMRX-CT97-0122. JBK was supported in part by NSF grant PHY-0102409. The computer simulations were done on the Cray SV1’s at NERSC, the Cray T90 at NPACI, and on the SGI Origin 2000 at the University of Wales Swansea.

References

- [1] S.R. Amendolia *et al.*, Phys. Lett. **B146**, 116, (1984).
- [2] B. Velikson and D. Weingarten, Nucl. Phys. **B 249**, 433 (1985).
- [3] S. Gottlieb, in *Advances in Lattice Gauge Theories*, World Scientific, 1985;
 S. Huang, J. Negele and J. Polonyi, Nucl. Phys. **B 307**, 669, (1988);
 T.A. DeGrand and R.D. Loft, Phys. Rev. **D38**, 954 (1988);
 M.-C. Chu, M. Lissia and J. Negele, Nucl. Phys. **B 360**, 31 (1991);
 M. Hecht *et al.*, Phys. Rev. **D47**, 285 (1993).
- [4] M. Hecht and T.A. DeGrand, Phys. Rev. **D46**, 2155 (1992).
- [5] C. DeTar, Phys. Rev. **D32**, 276 (1985); **D37**, 2328 (1988).
- [6] Ph. de Forcrand *et al.*, Phys. Rev. **D63**, 054501 (2001).
- [7] T. Hatsuda and T. Kunihiro, Phys. Rev. Lett. **55**, 158 (1985).
- [8] C. Bernard *et al.*, Phys. Rev. Lett. **68**, 2125 (1992).
- [9] E. Laermann and P. Schmidt, Eur. Phys. J. **C20**, 541 (2001).
- [10] B. Rosenstein, B.J. Warr and S.H. Park, Phys. Rep. **205**, 59 (1991).
- [11] S.J. Hands, A. Kocić and J.B. Kogut, Ann. Phys. **224**, 29 (1993).
- [12] S.J. Hands, S. Kim and J.B. Kogut, Nucl. Phys. **B442**, 364 (1995).

- [13] I.M. Barbour, S.J. Hands, J.B. Kogut, M.-P. Lombardo and S.E. Morrison, Nucl. Phys. **B558**, 327 (1999).
- [14] K.G. Klimenko, Z. Phys. **C37**, 457 (1988);
 B. Rosenstein, B.J. Warr and S.H. Park, Phys. Rev. **D39**, 3088 (1989);
 S.J. Hands, A. Kocić and J.B. Kogut, Nucl. Phys. **B390**, 355 (1993);
 A. Kocić and J.B. Kogut, Nucl. Phys. **B455**, 229 (1995);
 S.J. Hands and S.E. Morrison, Phys. Rev. **D59**:116002 (1999);
 J.B. Kogut and C.G. Strouthos, Phys. Rev. **D63**:054502 (2001);
 S.J. Hands, B. Lucini and S.E. Morrison, Phys. Rev. Lett. **86**, 753 (2001);
 hep-lat/0109001.
- [15] J.B. Kogut, M.A. Stephanov and C.G. Strouthos, Phys. Rev. **D58**:096001 (1998);
 S.J. Hands, J.B. Kogut and C.G. Strouthos, Phys. Lett. **B515**, 407 (2001).
- [16] J. Clowser and C.G. Strouthos, hep-lat/0110136, *Applications of Maximum Entropy Method to Dynamical Fermions*;
 C.R. Allton, J. Clowser, S.J. Hands, J.B. Kogut and C.G. Strouthos, work in progress.
- [17] R. Gupta, G. Guralnik, G.W. Kilcup and S.R. Sharpe, Phys. Rev. **D43**, 2003 (1991).
- [18] C.J. Burden and A.N. Burkitt, Europhys. Lett. **3**, 545 (1987);
 L. Del Debbio, S.J. Hands and J.C. Mehegan, Nucl. Phys. **B502**, 269 (1997).
- [19] L. Kärkkäinen, R. Lacaze, P. Lacey and B. Petersson, Nucl. Phys. **B415**, 781 (1994),
erratum Nucl. Phys. **B438**, 650 (1995);
 E. Focht, J. Jersák and J. Paul, Phys. Rev. **D53**, 4616 (1996).
- [20] M. Modugno, G. Pettini and R. Gatto, Phys. Rev. **D57**, 4995 (1998).
- [21] H.A. Weldon, Phys. Rev. **D40**, 2410 (1989).
- [22] T.N. Tran, Ph.D. thesis, University of Illinois (unpublished).

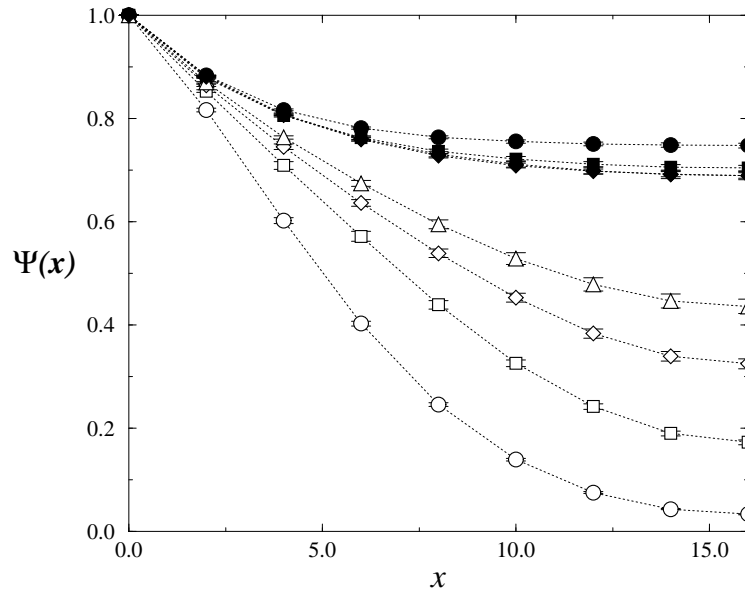


Figure 1: PS wavefunctions at $\beta = 0.55$. Filled symbols correspond to wall source; t increases from top to bottom. Empty symbols correspond to point source; t increases from bottom to top.

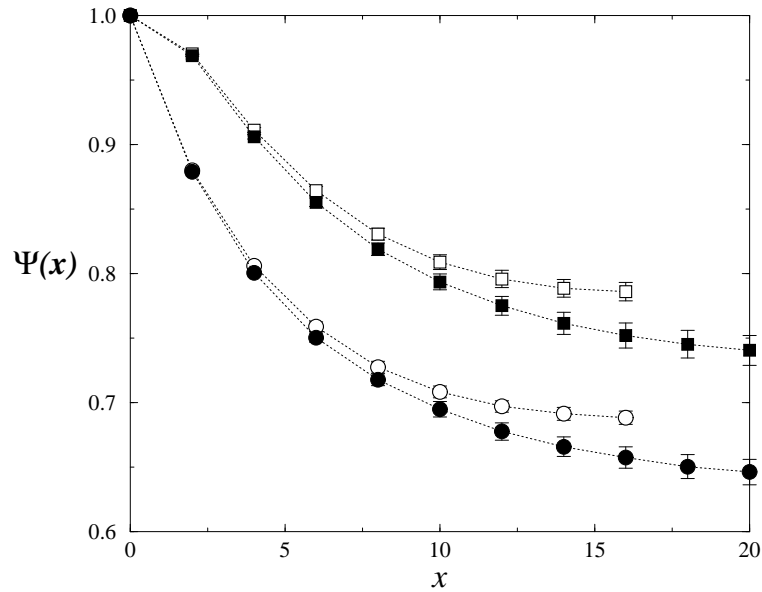


Figure 2: S and PS wavefunctions at $\beta = 0.55$ and $L_s = 32, 48$.

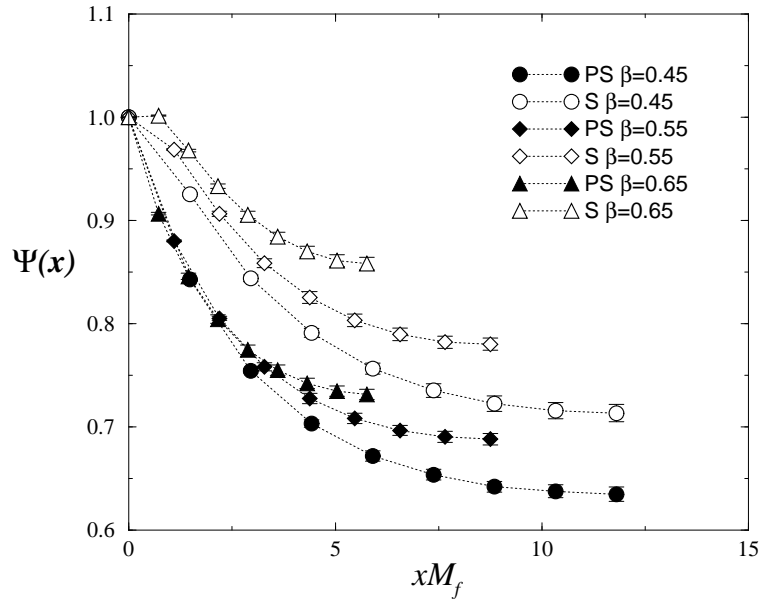


Figure 3: S and PS wavefunctions at $\beta = 0.45, 0.55, 0.65$; the horizontal axis is rescaled by the fermion mass M_f .

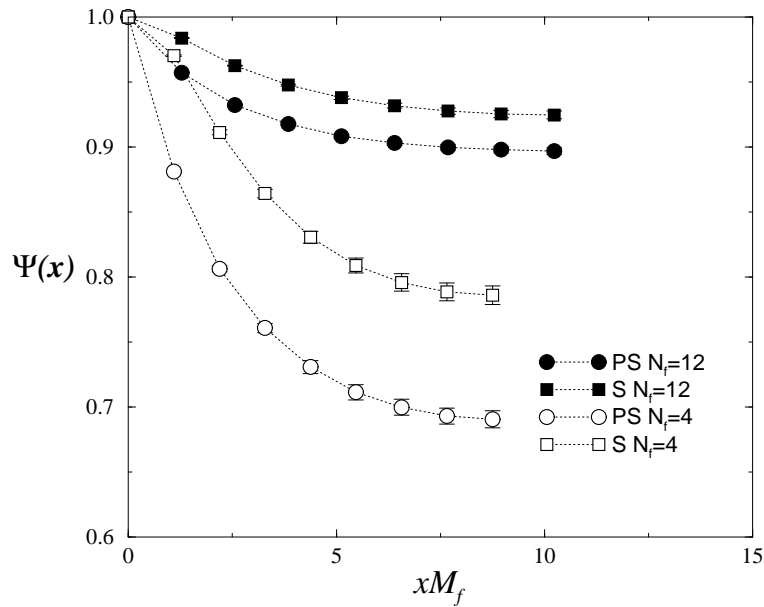


Figure 4: S and PS wavefunctions for $N_f = 4$ and $N_f = 12$; the horizontal axis is rescaled by M_f .

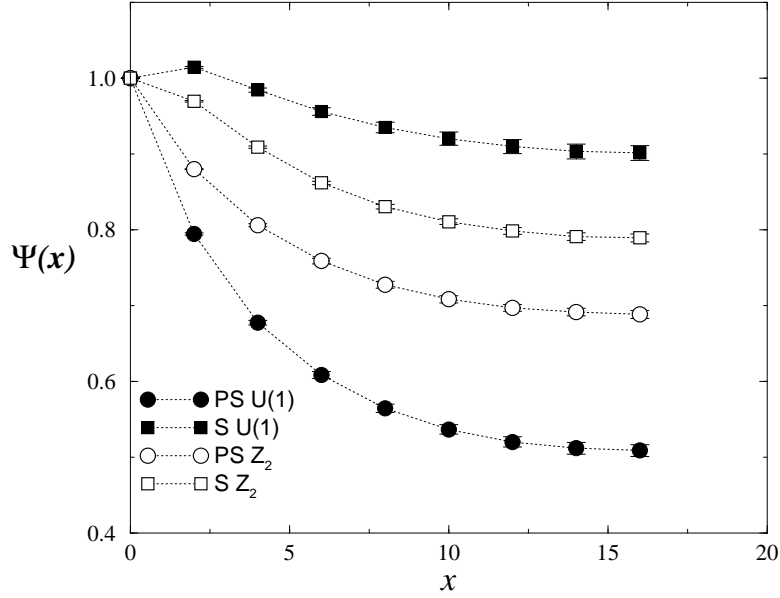


Figure 5: S and PS wavefunctions from the $U(1)$ and Z_2 GNM₃.

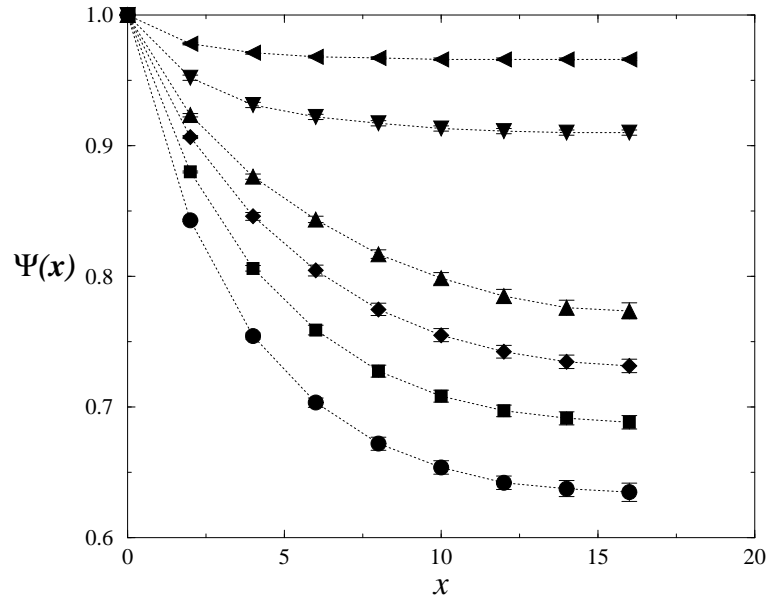


Figure 6: PS_{dir} wavefunctions in the broken phase ($\beta = 0.45, 55, 65, 0.75$) and in the symmetric phase ($\beta = 1.0, 2.0$); β increases from the bottom to the top of the figure.

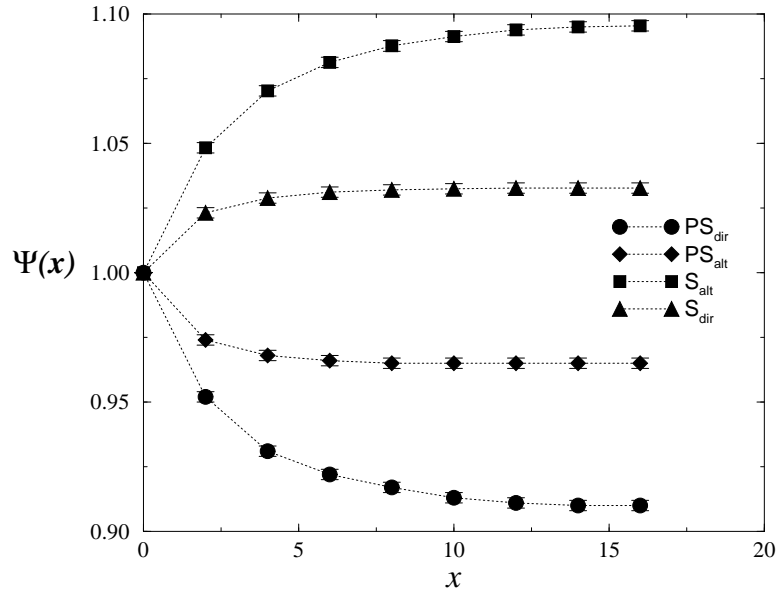


Figure 7: S and PS wavefunctions in the zero temperature symmetric phase.

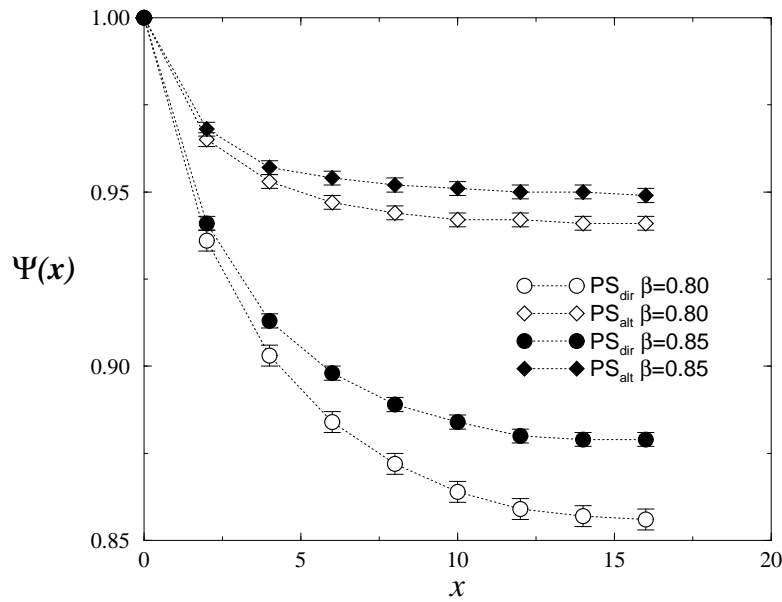


Figure 8: PS wavefunctions in the high T symmetric phase.

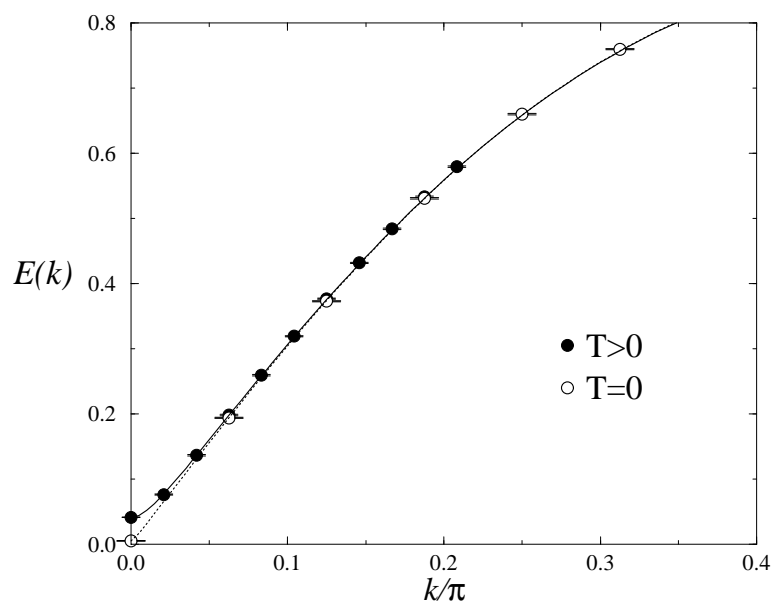


Figure 9: Fermion dispersion relations at $T = 0$ and $T > 0$.